THE JOURNAL OF PHYSICAL CHEMISTRY LETTERS
A JOURNAL OF THE AMERICAN CHEMICAL SOCIETY

pubs.acs.org/JPCL

Letter

Ground-State Orbital Analysis Predicts S_1 Charge Transfer in Donor−Acceptor Materials

Ali Abou Taka, John M. Herbert, and Laura M. McCaslin*

Cite This: *J. Phys. Chem. Lett.* 2023, 14, 11063−11068

Read Online

ACCESS | Metrics & More | Article Recommendations | Supporting Information

ABSTRACT: Donor−acceptor (D−A) materials can exhibit a wide range of unique photophysical properties with applications in next-generation optoelectronics. Electronic structure calculations of D−A dimers are often employed to predict the properties of D−A materials. One of the most important D−A dimer quantities is the degree of charge transfer (DCT) in the S_1 state, which correlates with properties such as fluorescence lifetimes and intersystem crossing rates in D−A materials. While predictive metrics of the S_1 DCT generally require an excited-state quantum chemistry calculation, presented here is a novel metric that predicts S_1 DCT solely with ground-state orbital analysis. This metric quantifies the similarity of the orbitals between a dimer complex and its monomer components. A linear relationship is found between this similarity metric and the S_1 DCT, calculated using a data set of 31 D−A dimers. Best practices for integrating this novel orbital structure−function relationship into high-throughput screening methods are discussed.

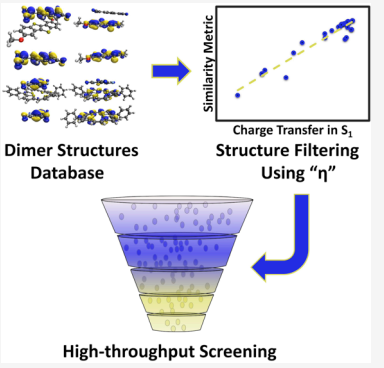

In the search for next-generation optoelectronic devices, there has been a growing interest in donor−acceptor (D−A) materials, including D−A co-crystals, for their application in organic solar cells and organic light-emitting diodes.[1−3] D−A complexes, by definition, exhibit charge transfer (CT) in their ground state and select excited states.[4] In the search for structure−function relationships to integrate into high-throughput screening and machine learning protocols,[5−9] several studies have assessed ways to predict the degree of CT (DCT), or ionicity parameter, in the S_0 state of D−A materials from molecular quantities such as orbital energies, vibrational frequencies, and geometric parameters.[10−14] Early evidence shows a relationship between DCT in S_0 to the magnitude of effective CT integrals,[11] commonly used in models of charge transport.[13−18] The DCT in the first electronically excited state of D−A dimers, S_1, has emerged as a key quantity for predicting radiative and nonradiative lifetimes in D−A materials, including intersystem crossing rates and fluorescence lifetimes.[2,19−23] These lifetimes are particularly difficult to compute directly using D−A dimer models, as energy levels and transition dipoles often differ substantially between the molecular cluster and material.[24,25]

A variety of DCT metrics for excited-state calculations have been put forward, as reviewed recently.[26,27] A widely used example is the "Λ metric" introduced by Peach et al.[28] as a diagnostic for time-dependent density functional theory calculations. The definition of Λ is based on spatial overlaps of occupied and virtual orbitals, evaluated by numerical quadrature and weighted by excitation amplitudes, but importantly, this and other standard DCT metrics require an excited-state calculation. Here, we consider whether ground-state orbital overlaps are sufficient for indicating CT character in the $S_0 \rightarrow S_1$ transition.

We construct a similarity metric, η, as follows. First, we define a molecular orbital (MO)

$$|\phi_i\rangle = \sum_\mu C_{\mu i} |\chi_\mu\rangle \tag{1}$$

where ϕ_i is the sum of atomic basis functions χ_μ with MO coefficients $C_{\mu i}$. We compute the overlap O_{ij} between the MOs ϕ_i and $\tilde{\phi}_j$, where $\tilde{\phi}_j$ uses the same atomic basis functions as ϕ_i at a displaced geometry. This overlap is

$$O_{ij} = \langle \phi_i | \tilde{\phi}_j \rangle = \sum_{\mu\nu} C_{\mu i} S_{\mu\nu} \tilde{C}_{\nu j} \tag{2}$$

where $S_{\mu\nu} = \langle \chi_\mu | \tilde{\chi}_\nu \rangle$ is the overlap matrix involving displaced basis functions. We compute O_{ij} twice: once between the HOMO (highest occupied molecular orbital) of the isolated donor molecule (HOMO^i) and the HOMO of the donor molecule within the complex (HOMO^c), using ghost functions to ensure that both calculations have the same basis functions; and second, between the LUMO (lowest unoccupied molecular orbital) of the isolated acceptor molecule (LUMO^i) and the LUMO of the acceptor molecule within

Received: October 8, 2023
Revised: November 25, 2023
Accepted: November 27, 2023

https://doi.org/10.1021/acs.jpclett.3c02787
J. Phys. Chem. Lett. 2023, 14, 11063−11068

the complex (LUMO^c). We define η as the average of these two quantities:

$$\eta = \frac{1}{2}(O_{\mathrm{HOMO}^i,\mathrm{HOMO}^c} + O_{\mathrm{LUMO}^i,\mathrm{LUMO}^c}) \quad (3)$$

The two geometries are oriented using the Kabsch algorithm[29] in order to maximize the overlap. Each computation of η requires three ground-state calculations: to obtain the orbitals of the isolated donor molecule, the orbitals of the isolated acceptor molecule, and the orbitals of the D−A complex. The calculation of O_{ij} is performed in a locally modified version of Q-Chem.[30]

To assess the correlation between η and the S_1 DCT of D−A dimers, we screened 31 D−A complexes with the donor and acceptor molecules shown in Figure 1, whose S_1 states are

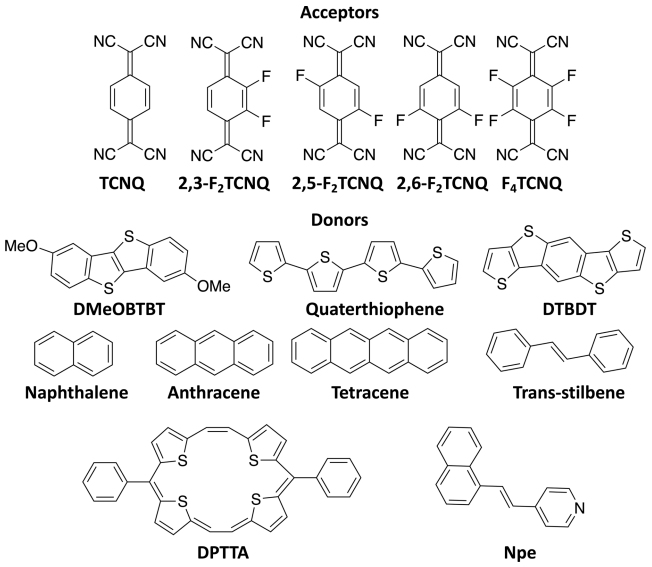

Figure 1. Chemical structures of the donor and acceptor molecules.

dominated by a HOMO → LUMO transition. The chosen donor and acceptor molecules are augmented from a data set recently chosen in a screening of S_0 DCT.[14] The donor molecules exhibit a diversity of molecular structures, while the acceptor molecules are 7,7,8,8-tetracyanoquinodimethane (TCNQ) and its fluorinated derivatives, F_xTCNQ. Geometries are optimized with Gaussian G16 at the CAM-B3LYP/6-31+G(d,p) level of theory with Grimme D3 dispersion.[28,31−33] Excited-state calculations were also carried out using CAM-B3LYP-D3/6-31+G(d,p) within the linear response time-dependent density functional theory (TDDFT) formalism.[26,34−36] We calculated the DCT using natural bond orbital (NBO) population analysis implemented in Gaussian G16 and transition density matrix (TDM) analysis in TheoDORE.[37,38]

We investigate the impact of geometries used to compute η by plotting η versus S_1 DCT in two ways. First, we optimize both the isolated monomers and their dimer complex and compute η versus S_1 DCT (Figure 2, top). Second, we optimize the dimer complex and take the geometries of the isolated monomers to be the same as those in their dimer complex (Figure 2, bottom). In each case, the S_1 DCT is computed by using TDM analysis. Notably, we observed significant variations in the η values when the monomers were optimized, as evidenced by the outliers shown in the top plot of Figure 2. The R^2 value from linear regression is 0.66 when

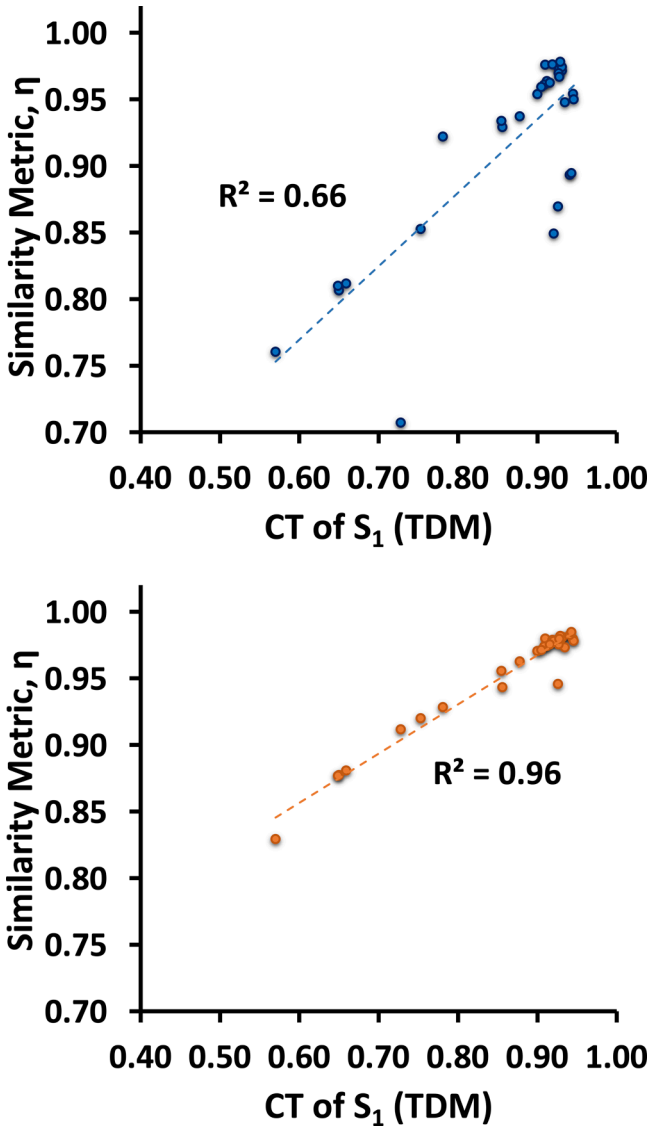

Figure 2. Plots of η versus S_1 DCT. Top: values computed at optimized monomer geometries and optimized dimer geometries. Bottom: values computed at the optimized dimer geometries only.

comparing optimized monomers versus optimized dimers, while the R^2 value is 0.96 when monomer geometries are unrelaxed from those found in the dimer complex. In both cases, our analysis reveals a positive linear correlation between the S_1 DCT and η, indicating that the S_1 DCT is large when the HOMO (LUMO) orbital of the donor (acceptor) retains its character from the isolated molecule. To assess the underlying reasons for the impact of the geometry choice on the evaluation of η, we plot the change in the average atomic root mean square deviation (RMSD) between geometries alongside the absolute difference in η, as shown in the Supporting Information, Figure S1. We show a correlation between the average atomic RMSD and absolute difference in η, indicating that the orbital character is likely to change most when the relaxed monomer geometries are significantly different from the geometries they assume in the dimer complex.

There are certain practical advantages that arise with the finding that the unrelaxed monomer geometries provide superior performance, including the elimination of the

https://doi.org/10.1021/acs.jpclett.3c02787
J. Phys. Chem. Lett. 2023, 14, 11063−11068

computational cost associated with optimizing the monomer geometries. Moreover, computing η at a single geometry eliminates the necessity of evaluating the atomic overlap integrals at displaced geometries. This simplifies the calculation of η, as $S_{\mu\nu}$ becomes the atomic basis self-overlap matrix, which is commonly printed in the output of electronic structure programs.[31]

To assess the sensitivity of η to the dimer geometry, thus bridging the gap between D−A dimers and D−A co-crystals, we perform an analysis of the S_1 DCT versus η for geometries from experimental crystallographic data (where available) and compare these results to those found in Figure 2. S_1 DCT is again computed using TDM analysis. Figure 3 shows the

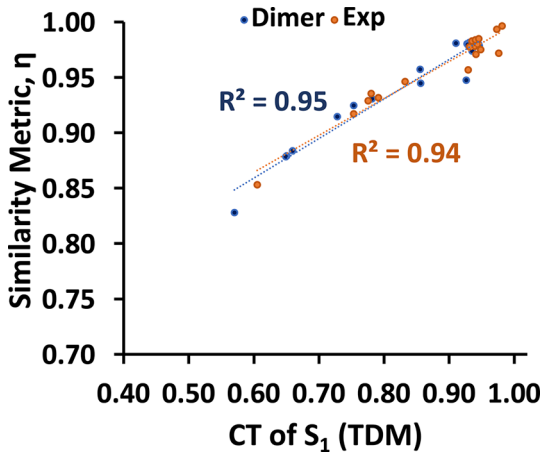

Figure 3. Plot of η versus S_1 DCT at the experimental crystal structures (orange) and optimized D−A dimer geometries (blue).

results obtained using the geometries from the experimental data in comparison to the dimer geometries, which indicate that the positive linear correlation still holds when the D−A geometries are taken from experimental crystal structures. In fact, when linear regressions are performed separately, the trend lines are almost indistinguishable. In Table 1, we report the value of η computed at each geometry (dimer complex versus experiment) and the percent deviation between the two. The values of η obtained from these two geometries have very small percent deviations, from 0.1% to 6% with an average of 1.3%. This shows that η can bridge between different types of molecular structures (isolated dimer and experimental crystal), indicating the reliability of the metric for different data sources. This is challenging for predictive metrics that rely on orbital energies.

We next assessed two methodologies for calculating the correlation of S_1 DCT with η. Using unrelaxed molecular geometries taken from the dimer complexes, Figure 4 plots η versus S_1 DCT using TDM analysis (as in Figure 2) as well as NBO analysis. The TDM-analyzed data (R^2 = 0.96) exhibits stronger correlation than the NBO-analyzed data (R^2 = 0.57). The poor fit in the latter case is due to the method's inability to treat delocalized electron transfer.[37] Conversely, TDM analysis provides a spatial mapping of the electron−hole pair associated with an electronic transition between two states and can successfully treat such delocalized electron transfer.[38,39] While both methods are commonly used to calculate the charges in molecules, we recommend TDM analysis over NBO analysis.

In the left panel of Figure 5, the HOMO for DMeO-BTBT, the LUMO for TCNQ, and the HOMO and LUMO of their

Table 1. η Values Using the Experimental Crystal (exp) and Dimer Geometries and the Percent Deviation (%D) of η_{dimer} from η_{exp}

system	η_{exp}	η_{dimer}	%D
4T:F_2TCNQ	0.932	0.945	1.4
4T:F_4TCNQ	0.917	0.931	1.5
4T:TCNQ	0.946	0.957	1.2
anthracene:F_4TCNQ	0.983	0.981	0.2
DMeO-BTBT:F_2TCNQ	0.975	0.980	0.5
DMeO-BTBT:F_4TCNQ	0.971	0.974	0.3
DMeO-BTBT:TCNQ[a]	0.957	0.948	1.0
DPTTA:25F_2TCNQ[a]	0.929	0.915	1.5
DPTTA:26F_2TCNQ	0.935	0.879	6.1
DPTTA:F_4TCNQ	0.853	0.828	3.0
DTBDT:F_2TCNQ	0.978	0.980	0.1
DTBDT:F_4TCNQ	0.972	0.975	0.3
DTBDT:TCNQ	0.980	0.981	0.1
naphthalene:TCNQ	0.997	0.975	2.1
Npe:TCNQ	0.993	0.985	0.9
STB:F_4TCNQ	0.978	0.964	1.4
STB:TCNQ	0.984	0.974	1.0
tetracene:F_4TCNQ	0.985	0.973	1.2
average %D			1.3

[a]Acceptor and donor molecules are perpendicular and do not interact via $\pi-\pi$ stacking.

dimer complex are visualized; this D−A dimer has the greatest S_1 DCT in the data set. The visual similarity between the monomer orbitals and those in the complex is apparent, and the localization onto the donor and acceptor moieties in the complex is striking. In the right panel of Figure 5, the HOMO of DPTTA, the LUMO of F_4TCNQ, and the HOMO and LUMO of their dimer complex are visualized; this D−A dimer has the smallest S_1 DCT in the data set. While there is significant visual similarity between the monomer MOs and those in the complex, there is also substantial delocalization of the HOMO onto the acceptor molecule and similar delocalization of the LUMO onto the donor. To maximize S_1 DCT, the electron density must be localized on the electron donor in the HOMO and transferred completely to the acceptor LUMO. The value of η quantifies the degree to which the isolated HOMO (LUMO) of the donor (acceptor) correlates with that in the complex, which predicts S_1 DCT.

We have shown that the S_1 (HOMO → LUMO) DCT can be predicted by a novel metric, η, that computes the average similarity between the donor (acceptor) molecule's HOMO (LUMO) and that of the corresponding orbital in the D−A complex. We found that η exhibits a positive linear correlation with the S_1 DCT for a set of 31 D−A pairs. In choosing molecular geometries to compute η, we found that by comparing the orbitals between isolated donor and acceptor molecules and their corresponding D−A complexes, one should use the same molecular geometries in the isolated molecules as in the D−A complex. Alternatively, experimental crystal structure data for the D−A complex can be used instead of optimized D−A dimer geometries. This allows flexibility in input data for inclusion in high-throughput screening and machine learning protocols. Lastly, we compared two methods for determining DCT, NBO analysis and TDM analysis, and found that TDM analysis is more reliable due to its ability to treat electron delocalization. Future work will aim to generalize the η metric to characterize the DCT of other electronic states

https://doi.org/10.1021/acs.jpclett.3c02787
J. Phys. Chem. Lett. 2023, 14, 11063−11068

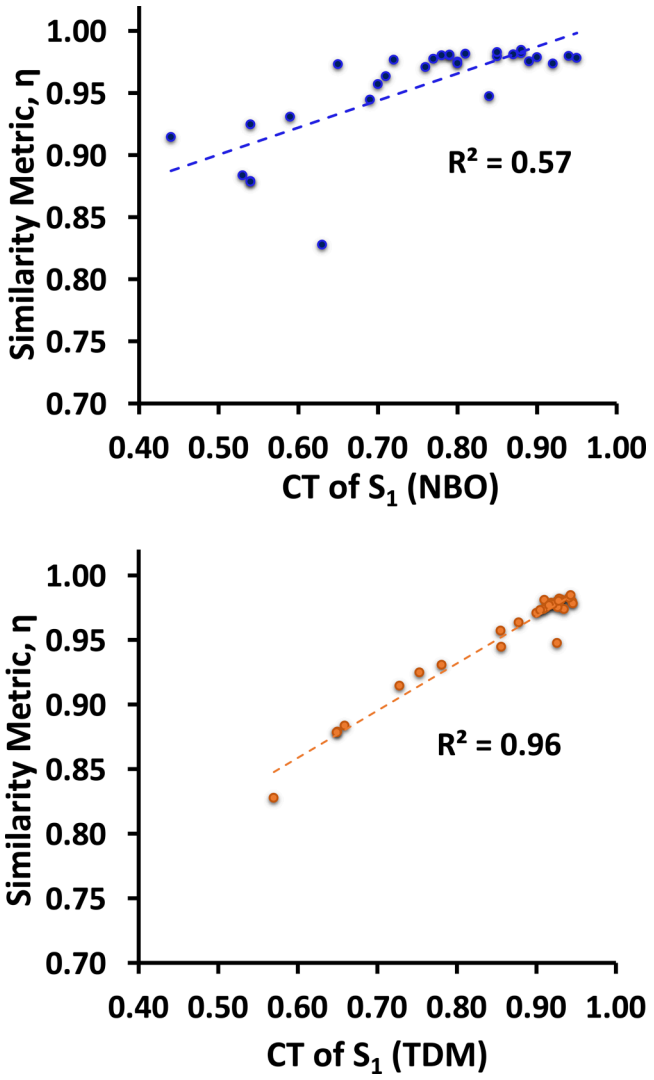

Figure 4. Plot of η versus S_1 DCT using NBO (top) and TDM (bottom) analyses at the D−A dimer geometries.

with the goal of uncovering further orbital structure−function relationships.

■ ASSOCIATED CONTENT

Supporting Information

A data repository of the calculations and code used in this work can be accessed free of charge at https://doi.org/10.6084/m9.figshare.24681261. The Supporting Information is available free of charge at https://pubs.acs.org/doi/10.1021/acs.jpclett.3c02787.

Plot of absolute difference in η along with average RMSD between monomer-optimized and dimer-optimized geometries (PDF)

■ AUTHOR INFORMATION

Corresponding Author

Laura M. McCaslin − *Sandia National Laboratories, Livermore, California 94550, United States;* orcid.org/0000-0002-6705-8755; Email: lmmccas@sandia.gov

Authors

Ali Abou Taka − *Sandia National Laboratories, Livermore, California 94550, United States;* orcid.org/0000-0003-0001-2813

John M. Herbert − *Department of Chemistry and Biochemistry, The Ohio State University, Columbus, Ohio 43210, United States;* orcid.org/0000-0002-1663-2278

Complete contact information is available at: https://pubs.acs.org/10.1021/acs.jpclett.3c02787

Notes

The authors declare the following competing financial interest(s): J.M.H. serves on the board of directors of Q-Chem Inc.

■ ACKNOWLEDGMENTS

The authors thank Dr. Varun Rishi for helpful feedback on the manuscript. This work was supported by the Laboratory Directed Research and Development program at Sandia National Laboratories. Sandia National Laboratories is a

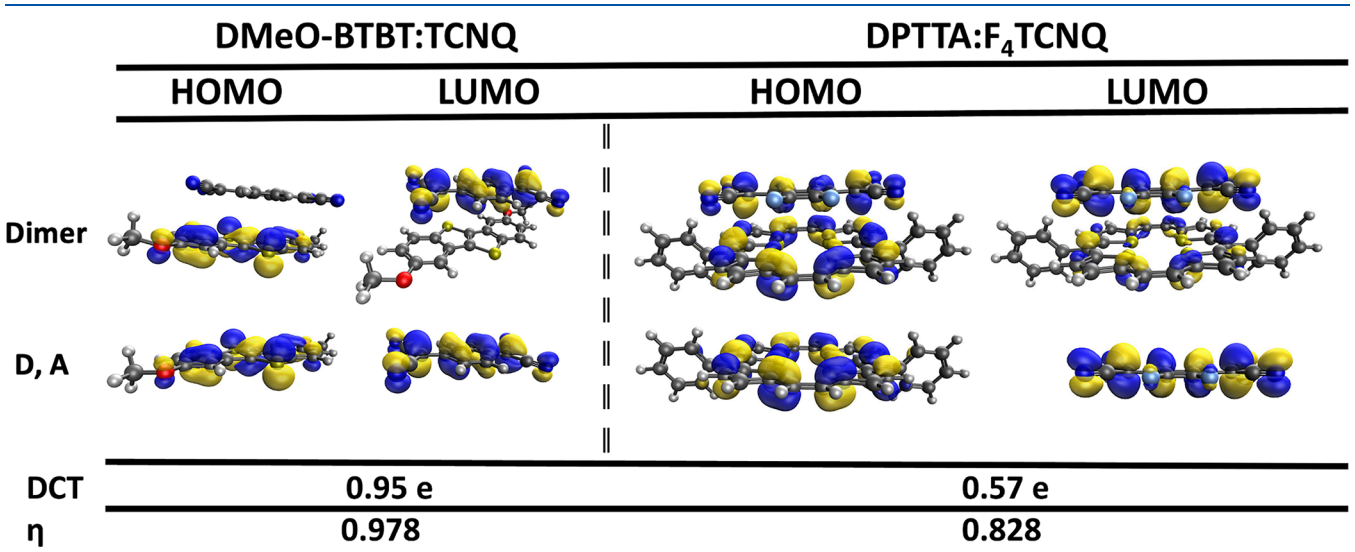

Figure 5. HOMO and LUMO for the D−A complex (top) and for the isolated molecules (bottom, donor at left and acceptor at right) using an isosurface value of 0.03 au. Associated S_1 DCT and η values are also shown.

multimission laboratory managed and operated by National Technology & Engineering Solutions of Sandia, LLC (NTESS), a wholly owned subsidiary of Honeywell International, Inc. for the U.S. Department of Energy's National Nuclear Security Administration (DOE/NNSA) under contract DE-NA0003525. This written work was authored by an employee of NTESS. The employee, not NTESS, owns the right, title, and interest in and to the written work and is responsible for its contents. Any subjective views or opinions that might be expressed in the written work do not necessarily represent the views of the U.S. Government. The publisher acknowledges that the U.S. Government retains a nonexclusive, paid-up, irrevocable, worldwide license to publish or reproduce the published form of this written work, or allow others to do so, for U.S. Government purposes. The DOE will provide public access to results of federally sponsored research in accordance with the DOE Public Access Plan. J.M.H. acknowledges the National Science Foundation Grant CHE-1955282.

REFERENCES

(1) Jiang, H.; Hu, P.; Ye, J.; Zhang, K. K.; Long, Y.; Hu, W.; Kloc, C. Tuning of the Degree of Charge Transfer and the Electronic Properties in Organic Binary Compounds by Crystal Engineering: A Perspective. *J. Mater. Chem. C* **2018**, *6*, 1884−1902.

(2) Lin, K.-H.; Wetzelaer, G.-J. A.; Blom, P. W.; Andrienko, D. Virtual Screening of TADF Emitters for Single-Layer OLEDs. *Front. Chem.* **2021**, *9*, 800027.

(3) Hernández, F. J.; Crespo-Otero, R. Modeling Excited States of Molecular Organic Aggregates for Optoelectronics. *Annu. Rev. Phys. Chem.* **2023**, *74*, 547−571.

(4) Mulliken, R. S. Molecular Compounds and Their Spectra. III. The Interaction of Electron Donors and Acceptors. *J. Phys. Chem.* **1952**, *56*, 801−822.

(5) Wu, Y.; Guo, J.; Sun, R.; Min, J. Machine Learning for Accelerating the Discovery of High-Performance Donor/Acceptor Pairs in Non-Fullerene Organic Solar Cells. *npj Comput. Mater.* **2020**, *6*, 120.

(6) Ju, C.-W.; Bai, H.; Li, B.; Liu, R. Machine Learning Enables Highly Accurate Predictions of Photophysical Properties of Organic Fluorescent Materials: Emission Wavelengths and Quantum Yields. *J. Chem. Inf. Model.* **2021**, *61*, 1053−1065.

(7) Mahmood, A.; Wang, J.-L. Machine Learning for High Performance Organic Solar Cells: Current Scenario and Future Prospects. *Energy Environ. Sci.* **2021**, *14*, 90−105.

(8) Rodríguez-Martínez, X.; Pascual-San-José, E.; Campoy-Quiles, M. Accelerating Organic Solar Cell Material's Discovery: High-Throughput Screening and Big Data. *Energy Environ. Sci.* **2021**, *14*, 3301−3322.

(9) Liu, X.; Shao, Y.; Lu, T.; Chang, D.; Li, M.; Lu, W. Accelerating the Discovery of High-Performance Donor/Acceptor Pairs in Photovoltaic Materials via Machine Learning and Density Functional Theory. *Mater. Des.* **2022**, *216*, 110561.

(10) Zhu, L.; Kim, E.-G.; Yi, Y.; Brédas, J.-L. Charge Transfer in Molecular Complexes with 2,3,5,6-Tetrafluoro-7,7,8,8-Tetracyanoquinodimethane (F_4-TCNQ): A Density Functional Theory Study. *Chem. Mater.* **2011**, *23*, 5149−5159.

(11) Behera, R. K.; Goud, N. R.; Matzger, A. J.; Brédas, J.-L.; Coropceanu, V. Electronic Properties of 1,5-Diaminonaphthalene: Tetrahalo-1,4-Benzoquinone Donor-Acceptor Cocrystals. *J. Phys. Chem. C* **2017**, *121*, 23633−23641.

(12) Zhuo, M.-P.; Yuan, Y.; Su, Y.; Chen, S.; Chen, Y.-T.; Feng, Z.-Q.; Qu, Y.-K.; Li, M.-D.; Li, Y.; Hu, B.-W.; Wang, X.-D.; Liao, L.-S. Segregated Array Tailoring Charge-Transfer Degree of Organic Cocrystal for the Efficient Near-Infrared Emission Beyond 760 nm. *Adv. Mater.* **2022**, *34*, 2107169.

(13) Zhu, L.; Yi, Y.; Li, Y.; Kim, E.-G.; Coropceanu, V.; Brédas, J.-L. Prediction of Remarkable Ambipolar Charge-Transport Characteristics in Organic Mixed-Stack Charge-Transfer Crystals. *J. Am. Chem. Soc.* **2012**, *134*, 2340−2347.

(14) Shi, W.; Deng, T.; Wong, Z. M.; Wu, G.; Yang, S.-W. A Molecular Roadmap Towards Organic Donor-Acceptor Complexes with High-Performance Thermoelectric Response. *npj Comput. Mater.* **2021**, *7*, 107.

(15) Zhang, J.; Geng, H.; Virk, T. S.; Zhao, Y.; Tan, J.; Di, C.-a.; Xu, W.; Singh, K.; Hu, W.; Shuai, Z.; Liu, Y.; Zhu, D. Sulfur-Bridged Annulene-TCNQ Co-crystal: A Self-Assembled "Molecular Level Heterojunction" with Air Stable Ambipolar Charge Transport Behavior. *Adv. Mater.* **2012**, *24*, 2603−2607.

(16) Vermeulen, D.; Zhu, L.; Goetz, K.; Hu, P.; Jiang, H.; Day, C.; Jurchescu, O.; Coropceanu, V.; Kloc, C.; McNeil, L. Charge Transport Properties of Perylene-TCNQ Crystals: The Effect of Stoichiometry. *J. Phys. Chem. C* **2014**, *118*, 24688−24696.

(17) Fonari, A.; Sutton, C.; Brédas, J.-L.; Coropceanu, V. Impact of Exact Exchange in the Description of the Electronic Structure of Organic Charge-Transfer Molecular Crystals. *Phys. Rev. B* **2014**, *90*, 165205.

(18) Qin, Y.; Cheng, C.; Geng, H.; Wang, C.; Hu, W.; Xu, W.; Shuai, Z.; Zhu, D. Efficient Ambipolar Transport Properties in Alternate Stacking Donor-Acceptor Complexes: From Experiment to Theory. *Phys. Chem. Chem. Phys.* **2016**, *18*, 14094−14103.

(19) Blaskovits, J. T.; Fumanal, M.; Vela, S.; Corminboeuf, C. Designing Singlet Fission Candidates from Donor-Acceptor Copolymers. *Chem. Mater.* **2020**, *32*, 6515−6524.

(20) Kim, J. H.; Yun, J. H.; Lee, J. Y. Recent Progress of Highly Efficient Red and Near-Infrared Thermally Activated Delayed Fluorescent Emitters. *Adv. Opt. Mater.* **2018**, *6*, 1800255.

(21) Zhu, Y.; Vela, S.; Meng, H.; Corminboeuf, C.; Fumanal, M. Donor-Acceptor-Donor "Hot Exciton" Triads for High Reverse Intersystem Crossing in OLEDs. *Adv. Opt. Mater.* **2022**, *10*, 2200509.

(22) Li, W.; Pan, Y.; Yao, L.; Liu, H.; Zhang, S.; Wang, C.; Shen, F.; Lu, P.; Yang, B.; Ma, Y. A Hybridized Local and Charge-Transfer Excited State for Highly Efficient Fluorescent OLEDs: Molecular Design, Spectral Character, and Full Exciton Utilization. *Adv. Opt. Mater.* **2014**, *2*, 892−901.

(23) Usta, H.; Cosut, B.; Alkan, F. Understanding and Tailoring Excited State Properties in Solution-Processable Oligo(p-Phenyleneethynylene)s: Highly Fluorescent Hybridized Local and Charge Transfer Character via Experiment and Theory. *J. Phys. Chem. B* **2021**, *125*, 11717−11731.

(24) Guerrini, M.; Valencia, A. M.; Cocchi, C. Long-Range Order Promotes Charge-Transfer Excitations in Donor/Acceptor Co-crystals. *J. Phys. Chem. C* **2021**, *125*, 20821−20830.

(25) Abou Taka, A.; Reynolds, J. E.; Cole-Filipiak, N. C.; Shivanna, M.; Yu, C. J.; Feng, P.; Allendorf, M. D.; Ramasesha, K.; Stavila, V.; McCaslin, L. M. Comparing the Structures and Photophysical Properties of Two Charge Transfer Co-crystals. *Phys. Chem. Chem. Phys.* **2023**, *25*, 27065−27074.

(26) Herbert, J. M. Density-Functional Theory for Electronic Excited States. In *Theoretical and Computational Photochemistry*; Elsevier Science, 2023; p 69−118.

(27) Herbert, J. M. Visualizing and Characterizing Excited States from Time-Dependent Density Functional Theory. *ChemRxiv* **2023**.

(28) Peach, M. J.; Benfield, P.; Helgaker, T.; Tozer, D. J. Excitation Energies in Density Functional Theory: An Evaluation and a Diagnostic Test. *J. Chem. Phys.* **2008**, *128*, 044118.

(29) Kabsch, W. A. Solution for the Best Rotation to Relate Two Sets of Vectors. *Acta Crystallographica Section A: Crystal Physics, Diffraction, Theoretical and General Crystallography* **1976**, *32*, 922−923.

(30) Epifanovsky, E.; et al. Software for the Frontiers of Quantum Chemistry: An Overview of Developments in the Q-Chem 5 Package. *J. Chem. Phys.* **2021**, *155* (8), 084801.

(31) Frisch, M. J., et al. In *Gaussian 16, Revision B.01*; Gaussian, Inc., Wallingford, Connecticut, U.S., 2016.

https://doi.org/10.1021/acs.jpclett.3c02787
J. Phys. Chem. Lett. 2023, 14, 11063−11068

(32) Yanai, T.; Tew, D. P.; Handy, N. C. A New Hybrid Exchange-Correlation Functional Using the Coulomb-Attenuating Method (CAM-B3LYP). *Chem. Phys. Lett.* **2004**, *393*, 51−57.
(33) Grimme, S.; Ehrlich, S.; Goerigk, L. Effect of the Damping Function in Dispersion Corrected Density Functional Theory. *J. Comput. Chem.* **2011**, *32*, 1456−1465.
(34) Bauernschmitt, R.; Ahlrichs, R. Treatment of Electronic Excitations Within the Adiabatic Approximation of Time Dependent Density Functional Theory. *Chem. Phys. Lett.* **1996**, *256*, 454−464.
(35) Casida, M. E.; Jamorski, C.; Casida, K. C.; Salahub, D. R. Molecular Excitation Energies to High-Lying Bound States from Time-Dependent Density-Functional Response Theory: Characterization and Correction of the Time-Dependent Local Density Approximation Ionization Threshold. *J. Chem. Phys.* **1998**, *108*, 4439−4449.
(36) Stratmann, R. E.; Scuseria, G. E.; Frisch, M. J. An Efficient Implementation of Time-Dependent Density-Functional Theory for the Calculation of Excitation Energies of Large Molecules. *J. Chem. Phys.* **1998**, *109*, 8218−8224.
(37) Glendening, E. D.; Reed, A. E.; Carpenter, J. E.; Weinhold, F. In *The NBO3.0 Program*; University of Wisconsin, Madison, Wisconsin, U.S., 2001.
(38) Plasser, F. TheoDORE: A Toolbox for a Detailed and Automated Analysis of Electronic Excited State Computations. *J. Chem. Phys.* **2020**, *152* (8), 084108.
(39) Li, Y.; Ullrich, C. Time-Dependent Transition Density Matrix. *Chem. Phys.* **2011**, *391*, 157−163.

https://doi.org/10.1021/acs.jpclett.3c02787
J. Phys. Chem. Lett. 2023, 14, 11063−11068